Chaos-Based Turbo Systems in Fading Channels

Francisco J. Escribano, *Member, IEEE*, Alexandre Wagemakers, and Miguel A. F. Sanjuán

***Abstract*—The growing demand for ubiquitous wireless communication services requires powerful coding and modulation schemes to counteract the signal degradation in the air interface, preferably without resorting to costly hardware. Previous work has demonstrated that chaos-based coded modulations could be robust in the flat fading channel. This paper illustrates that, as the flat fading channel quality degrades, parallel concatenated chaos-based coded modulations can provide better error performance than non-chaotic counterparts. Therefore, this joint coding and modulation approach may contribute to power saving in common adverse channel conditions. Moreover, it is shown that it is possible to manage its spectral efficiency while keeping its robustness under fading.**

***Index Terms*—Chaos, concatenated coding, error analysis, iterative decoding.**

I. Introduction

THE possibility of using chaotic signals to carry information was first introduced in the early 1990s [1]. At the beginning, this became a hot topic in nonlinear science and engineering because chaotic signals were considered to provide good properties for a number of important applications. For example, the uncorrelation and unpredictability properties of chaotic sequences seemed to be appropriate for secure communications or multiple access systems, thus promoting a great deal of research [2]. However, this interest decayed because many of the systems proposed were not so competitive as expected [3].

As a contrast with this situation, we have witnessed during the past decade the publication of some proposals competitive to the state-of-the-art standard systems. Some works, for example, ascertain the possibilities of chaos in secure communications [4], [5]. Chaos-based systems working at the waveform level have already shown to be of potential use in multipath fading channels [6]–[9], while chaos-based systems working at the coding level [10]–[12] behave well in multiuser channels. Other publications have stressed the fact that chaos-based coded modulated (CCM) systems working at a joint waveform and coding level can be specially efficient under additive white Gaussian noise (AWGN) [13]–[17]. These CCM systems have as well proved to be of potential interest in some classes of dispersive channels, as under flat fading [18], or intersymbol interference [19].

The extraordinary development of successful chaos-based communications has been enabled by the building of a comprehensive bridge linking the fields of chaos theory and digital communications. Some key achievements rely on the equivalent trellis encoder view of a family of CCM systems [13], [20], [21]. The related trellis coding and decoding steps give the possibility to design parallel concatenated CCM (PCCCM) systems exhibiting coding gains comparable to those achieved with standard binary parallel concatenated systems [14]. This has led very recently to the proposal of serially concatenated systems with promising performances [16]. Using concatenated coding and iterative decoding opens the road to practical applications, by taking advantage of one of the main strategies preferred nowadays to improve performance without increasing too much the processing requirements [22].

On the other hand, wireless communications keep focusing much of the research effort in the area due to the overall deployment of 3G and 4G networks. Therefore, there is a growing demand for higher throughputs in very low reliable air interfaces, which are adversely affected by such inconveniences as fading, Doppler effects and the like [23]. As it has been mentioned, CCM blocks used individually possess some interesting properties in frequency non-selective fast fading channels [18]. This, together with the fact that PCCCM systems yield performances comparable to more standard concatenated systems [14], gives a promising perspective to the employment of PCCCM under flat fading. PCCCM may not be a clear match for binary turbocodes or turbo trellis coded modulation (TTCM) systems [24] in AWGN. However, as the line-of-sight (LOS) component of the signal vanishes and the transmission is progressively effectuated through the dispersive component (transition from a Rician to a Rayleigh flat fading channel [25]), PCCCM can provide better bit error rate (BER). It is worth noting that one of the drawbacks of the CCM systems is the difficulty to manage spectral efficiency, since they basically work at an individual rate of 1 symbol per input bit. We show here that puncturing can help to introduce a higher spectral efficiency while still providing a good balance between degradation and coding gain.

According to all this, in Section II, we briefly review the main aspects of the chaos-based system setup. In Section III we provide analytic insight on the behavior of such systems, their potential advantages and trade-offs, by characterizing error floor bounds and mutual information transfer plots. In Section IV we give extensive simulation results and discuss the possibilities of the proposed systems as compared with well understood and practical counterparts, such as binary turbocodes and TTCM systems. Section V is devoted to the conclusions.

II. System Description

The PCCCM systems considered here are of the same kind as the ones proposed in [14], based on the CCM blocks analyzed in [18] under flat fading. Therefore, we do not review them in full detail, and only recall the main definitions. We will add a

Manuscript received March 21, 2013; revised May 27, 2013; accepted June 10, 2013. Date of publication September 09, 2013; date of current version January 24, 2014. This work was supported by the Spanish Ministerio de Ciencia e Innovación under Project No. FIS2009-09898, and from Spanish Ministerio de Economía y Competitividad, under Project No. TEC2012-38058-C03-01. This paper was recommended by Associate Editor Y. Uwate.

F. J. Escribano is with the Department of Signal Theory and Communications, Universidad de Alcalá, Escuela Politécnica Superior, 28805 Alcalá de Henares, Spain (e-mail: francisco.escribano@ieee.org).

A. Wagemakers and M. A. F. Sanjuán are with the Physics Department, Universidad Rey Juan Carlos, 28933 Móstoles, Spain (e-mail: alexandre.wagemakers@urjc.es; miguel.sanjuan@urjc.es).

Digital Object Identifier 10.1109/TCSI.2013.2278349

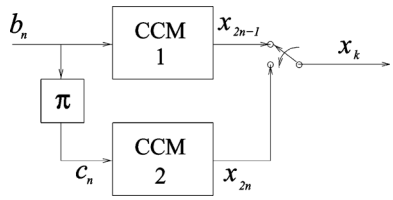

Fig. 1. Scheme of the unpunctured concatenated coded modulator.

new feature for this kind of CCM systems, the *phase mapping* of the symbols, which will prove to provide advantages.

A. Parallel Concatenated Encoder

The concatenated encoder consists in two CCM subsystems which accept as input successive blocks of N bits, $\mathbf{b} = \{b_1, \ldots, b_N\}$ for one CCM and $\mathbf{c} = \{c_1, \ldots, c_N\}$ for the other, where $\mathbf{c}$ is the interleaved counterpart of $\mathbf{b}$. The first CCM produces a block of chaos encoded samples $x_{2n-1}, n = 1, \ldots, N$, at a rate of 1 sample per input bit, and the second CCM produces a second block of chaos encoded samples $x_{2n}, n = 1, \ldots, N$, at the same rate (see Fig. 1). The PCCCM outputs blocks of size $2N$ (total rate in this setup $R = 1/2$ bits per chaotic symbol). The interleaver kind considered here is the well known S-random interleaver [26].

As shown in Figs. 3 and 4, a CCM block outputs chaos-like samples z_n, obtained by an encoding process that can be described by an equivalent trellis (finite-state) encoder with 2^Q states, so that z_n is quantized over 2^Q values ($z_n \in S_Q = \{z^0, \ldots, z^{2^Q-1}\}$), uniformly distributed in the interval [0, 1]. Further details can be found in [14]. The key point is that, as there is a one-to-one correspondence between the finite-state machine state at time n and the output value z_n, the properties of the chaos-based sequence are kept regardless of the initial state of the finite-state machine process and the corresponding initial z_0 value. For convenience, this initial state is taken as the all-zero value, so that it is known at the decoding stage to properly initialize it, as it will be shown in the Subsection devoted to the iterative decoder. Note how a CCM block consists of Q binary memory positions (r_i in the picture), a weighted sum of their contents, and a feedback loop to ensure the interleaver coding gain. We denote the CCM encoder state as $s_i \in \{s_0, \ldots, s_{2^Q-1}\}$, so that $s_i \leftrightarrow z^i \in S_Q$.

The x_n chaos encoded sample is obtained by mapping the z_n value from the interval [0, 1] to a more convenient set of values, in order to adapt better to the channel characteristics, as shown in Fig. 2. We have chosen these two possibilities:

- Amplitude mapping, where the [0, 1] interval is mapped symmetrically to the $[-1, 1]$ interval:

$$x_n = 2z_n - 1. \tag{1}$$

- Phase mapping, where the values in [0, 1] are used to drive the phase in the interval $[0, 2\pi]$ of a set of baseband-equivalent complex-valued samples with normalized amplitude:

$$x_n = e^{2\pi j z_n}. \tag{2}$$

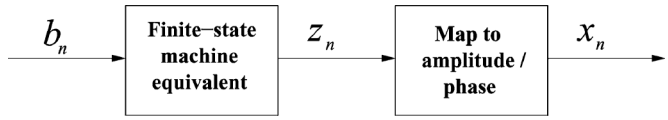

Fig. 2. CCM as a combination of a finite-state machine core and a mapper.

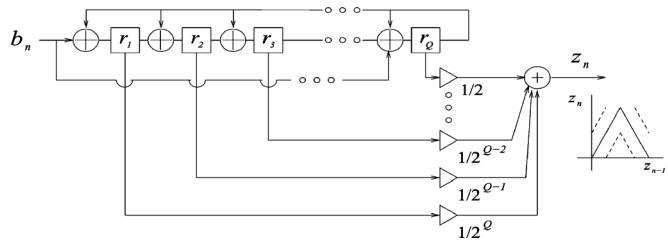

Fig. 3. Finite-state machine equivalent of an mTM CCM.

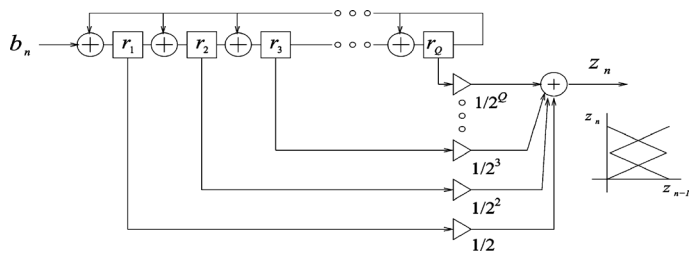

Fig. 4. Finite-state machine equivalent of an ImTM CCM.

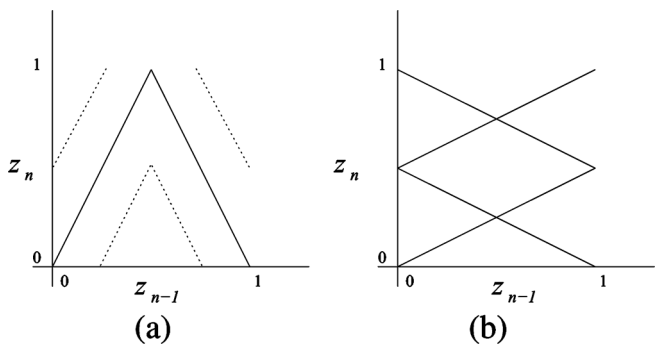

Fig. 5. Maps for the main constituent CCM encoders. (a) mTM; (b) ImTM.

This latter kind of mapping had not been applied before to the CCM systems used here, so that it is a novel approach. In the results section, we will verify that phase mapping can help to get significant gains.

The main CCM building blocks considered in our examples are the mTM (multi-tent map), and the ImTM (inverse multi-tent map), whose corresponding finite-state machine equivalent and underlying maps are shown in Figs. 3, 5(a), 4, and 5(b), respectively. The details and definitions can be found in [14], (4), (5), and (6). We provide also comparisons using other CCM systems, such as the multi-Bernoulli shift map (mBSM) and the tent map (TM). All these CCM building blocks have been characterized and extensively used in previous research works [14], [18], and, therefore, we only provide results for some of their combinations. The combinations chosen serve to highlight properties and trade-offs. The objective is to get evidences of their competitive possibilities against standard counterparts, and establish their limitations, along with design and evaluation criteria.

B. Channel Model

We consider here the frequency non-selective fast flat fading channel, so that the signal arriving at the decoder side will be

$$r_k = a_k \cdot x_k + n_k, \quad k = 1, \ldots, 2N, \tag{3}$$

where n_k are samples of a complex AWGN process with power σ^2. The fading sample, a_k, corresponds to an uncorrelated Rician process with parameter K [27]. The amplitude $|a|$ of this fading process sequence is described by a Rician probability density function (pdf) given by

$$p(|a|) = 2|a|(1+K)e^{-|a|^2(1+K)-K} I_0(2|a|\sqrt{K(K+1)}),$$

where $I_0(\cdot)$ is the zeroth-order modified Bessel function of the first kind, K is the ratio of specular to diffuse energy [27], and $|a| \geq 0$. $K = 0$ corresponds to the Rayleigh case, and $K \to \infty$, to no fading. The mean and variance of $|a|$ are given by

$$\eta_{|a|} = \frac{1}{2}\sqrt{\frac{\pi}{1+K}} e^{-\frac{K}{2}} \left[(1+K) I_0\left(\frac{K}{2}\right) + K I_1\left(\frac{K}{2}\right)\right]$$
$$\sigma^2_{|a|} = 1 - \eta_a^2,$$

where $I_1(\cdot)$ is the first-order modified Bessel function of the first kind. Note that $E[|a|^2] = 1$, so that the signal to noise ratio at the receiver side is not affected, and comparisons are easily made as functions of E_b/N_0 and K. According to the channel model chosen, the phase of the fading process sequence $\angle(a)$ corresponds to a uniform random variable in the interval $[0, 2\pi)$. These expressions model a wireless setup where the fading channel is fully interleaved (uncorrelated fast fading samples) and the line of sight (LoS) component of the transmitted signal varies from null (Rayleigh case, $K = 0$) to no dispersed component ($K \to \infty$) [25].

C. Iterative Decoder

The block of received samples (3) is fed to an iterative decoder for further processing. We assume also some method to estimate the channel so that conditions of perfect channel state information (CSI) exist. The channel coefficients a_k are fed to the decoding blocks through the CSI port in Fig. 6. Let us briefly review the maximum *a posteriori* (MAP) decoding algorithm for the chaos-based soft-input soft-output (SISO) modules in said Fig. 6 [14]. If the first CCM encoder is initially at state s_i and an input bit b_n drives it at state s_j at time n, with associated output x_{2n-1}, the output log-probability ratio $\Lambda(b_n; \mathrm{O})$ is calculated as follows[1]

$$\begin{aligned}\Lambda(b_n;\mathrm{O}) &= \log\frac{p(b_n=1;\mathrm{O})}{p(b_n=0;\mathrm{O})} \\ &= \log\frac{\sum_{s_i \xrightarrow[b_n=1]{} s_j} \exp(\alpha_n(s_i) + \pi(x_{2n-1};\mathrm{I}) + \beta_n(s_j))}{\sum_{s_i \xrightarrow[b_n=0]{} s_j} \exp(\alpha_n(s_i) + \pi(x_{2n-1};\mathrm{I}) + \beta_n(s_j))},\end{aligned} \tag{4}$$

[1]In all the following, $(\cdot;\mathrm{O})$ denotes output values or probabilities, and $(\cdot;\mathrm{I})$, input values or probabilities.

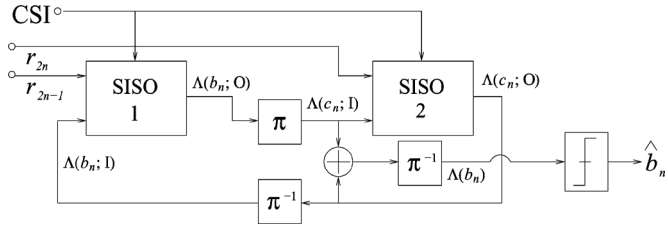

Fig. 6. Scheme of the iterative decoder.

where the summations are taken over all possible transitions $s_i \xrightarrow[b_n=b]{} s_j$ between pairs of states where the bit b_n takes the value $b \in \{0, 1\}$, and $n = 1, \ldots, N$. The quantities $\alpha_n(\cdot)$ and $\beta_n(\cdot)$ are the well known forward-backward log-probabilities of the MAP algorithm. The transition log-probability of the channel $\pi(x_{2n-1};\mathrm{I}) = \log[p(r_{2n-1}|x_{2n-1})]$ is the input metric for the algorithm, calculated as

$$\pi(x_{2n-1};\mathrm{I}) = A|r_{2n-1} - a_{2n-1} \cdot x_{2n-1}|^2 + B, \tag{5}$$

where A and B are constants which depend on the signal to noise ratio E_b/N_0 [14]. The second SISO can be described in the same way, just by writing c_n instead of b_n, x_{2n} instead of x_{2n-1}, and r_{2n} instead of r_{2n-1} (see Fig. 6). The initial state for the SISO algorithm is taken as the all-zero value, according to the initial state used in the CCM encoding process.

Once the iterative decoding algorithm is working in its intended way, the output probability estimations of one SISO decoder $(\Lambda(b_n;\mathrm{O}), \Lambda(c_n;\mathrm{O}))$ act as input probability estimations for the other one $(\Lambda(c_n;\mathrm{I}), \Lambda(b_n;\mathrm{I})$, after the interleaving and deinterleaving stages, respectively), until a fixed number of iterations is reached and a decision is made to get the block of decoded bits $\hat{b}_n, n = 1, \ldots, N$. Notice that the main difference of this algorithm with respect to the decoding algorithm of a standard binary turbocode lies in the fact that there are 2^Q possible different symbols in the channel to be accounted for when calculating the log transition metrics. In the case of TTCM, the main difference resides in the fact that they are intended to provide spectral efficiency with good BER down to the error floor region [24]. PCCCM systems lie somewhat in between.

D. Increasing Spectral Efficiency

As it has been shown, a CCM is a kind of TCM system with *a priori* no spectral efficiency, since it works at a rate of $R = 1$ symbol per bit, and therefore a PCCCM with two constituent CCM works at the rate of $R = 1/2$ symbol per bit. To increase efficiency and make PCCCM competitive with TTCM, puncturing is one of the most straightforward possibilities [24]. The puncturing chosen is different from the classical approach of puncturing bits at each component code: the quantized chaos-like sequence is punctured symbol-wise instead. An equivalent situation has been studied for TCM setups [28]. In our test cases, one symbol out of every two will be removed for each CCM, so that the block of symbols in the channel will have length N, corresponding to a block of input bits of length N. This allows a rate of $R = 1$ symbol per bit for the joint PCCCM. The operation on the symbol stream is depicted in Fig. 7, and corresponds to a puncturing pattern $p = (1, 0)$ [29].

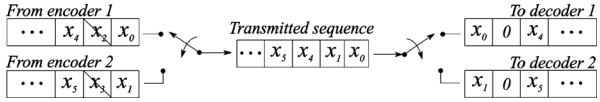

Fig. 7. Puncturing operation on the stream of symbols sent through the channel. The input for the decoder is represented as done for the phase mapping case.

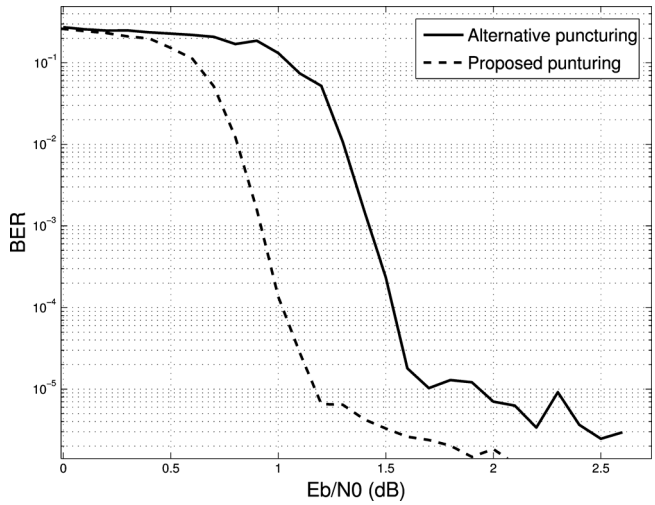

Fig. 8. Difference in the BER due to an alternative puncturing pattern.

This puncturing pattern is the most reasonable choice to optimize the spectral efficiency in the view of the chaotic paradigm. The correlation among the resulting chaotic-like sequences is preserved so as to ensure the correct decoding of the symbols with a limited amount of degradation. Moreover the statistics of the symbol stream in the channel are similar to the unpunctured case. In the results section, we will show that the comparative advantage of PCCCM under Rayleigh flat fading are kept even when punctured. From the point of view of the finite state machine, skipping more than one symbol implies more uncertainty and more divergence while decoding the punctured symbols. Any other choice (as for example skipping all symbols from one of the CCM blocks), would lead to a serious loss of information.

A similar puncturing approach has been proposed by Robertson *et al.* for a TTCM system [29], although the motivation for their choice is somehow different. We cannot supply exhaustive simulations of all the possible puncturing sequences. However, in order to illustrate the comparative advantage of skipping only one symbol out of every two consecutive ones, we have performed a simulation with a different puncturing pattern. In this case, the bandwidth efficiency is again 1 bit per channel use. The alternative puncturing sequence is given by the pattern $p = (1, 0, 0, 1)$, where two symbols out of four consecutive have been punctured. This leads to three transitions in each CCM decoding trellis affected by uncertainty. The resulting BER is obviously worse leading to a loss of 0.5 dB for the same bit error rate target, as seen in Fig. 8. If we focus on the chaotic dynamic of the underlying map, this is explained because sequences with close initial values diverge exponentially when iterated through the map, and so it is not convenient to skip more than one consecutive symbol in order to control the resulting degradation.

With respect to the modifications needed at the decoding stage to account for the punctured symbols, the new decoder is quite easy to implement just by weighting the probabilities of the removed transitions with equal probability metric values, while basically keeping the SISO structure unaffected [29]. In the case of phase mapping, this is done straightforwardly by introducing null dummy symbols in the place of the punctured ones, as shown in Fig. 7. This dummy symbol has equal distance with respect to any possible symbol at the output of each CCM, and therefore it leads naturally to equal metrics. In the case of amplitude mapping, the punctured symbol is forced to have $1/2^Q$ probability metric in the trellis, since there are 2^Q possible symbol values. Once this is done, the SISO decoder works as with unpunctured sequences. As stated, we will see that, although there is some loss with respect to the $R = 1/2$ case, there is still a gain in comparison with similar TTCM systems, specially under flat fading.

III. System Analysis

Concatenated systems with iterative decoding can be well characterized by studying their decoding convergence properties (mutual information transfer through density evolution) and their bit error limits (error floor) [24].

A. Bounding the Error Floor

The behavior of the individual CCM systems in an uncorrelated flat fast fading channel affected by AWGN is analyzed in [18], for the case of amplitude mapping of the chaos-based z_n samples (1). We will recall here the main results, adapt them without loss of generality to phase mapping (2), and draw the bounds for the error floor region of the parallel concatenation of two CCMs. Given that the original binary sequence $\mathbf{b}$ takes equiprobable values 0 and 1, we can assume, for high E_b/N_0 (i.e., in the error floor region), that the iterative decoding yields results equivalent to a proper maximum likelihood (ML) decoding based on the metrics described in (5). In this case, a $\mathbf{b}'$ erroneous sequence is decoded when its associated $\mathbf{x}'$ chaos-based sequence meets

$$\sum_{i=1}^{P} |r_i - a_i \cdot x_i|^2 > \sum_{j=1}^{P} \left|r_j - a_j \cdot x'_j\right|^2, \tag{6}$$

where P is either N or $2N$ for the punctured and unpunctured cases, respectively. It is easy to see that, following the approach of [18] adapted for complex valued samples and taking into account that $|a_i|$ follows a Rician pdf with parameter K, the pairwise error probability (PEP) given $\mathbf{x}$ and $\mathbf{x}'(P_e(\mathbf{x} \to \mathbf{x}'|\mathbf{x}))$ is as shown in (7), where R is the abovementioned rate in bits/symbol of the PCCCM, and $E_{\mathbf{a}}[\cdot]$ is the mathematical expectancy with respect to the fading coefficients.

$$\begin{aligned} P_e(\mathbf{x} \to \mathbf{x}'|\mathbf{x}) &= E_{\mathbf{a}}[P_e(\mathbf{x} \to \mathbf{x}'|\mathbf{x}, \mathbf{a})] \\ &\le \frac{1}{2} \prod_{i=1}^{P} \frac{1+K}{1+K+\frac{R}{4P}\frac{E_b}{N_0}|x_i - x'_i|^2} \\ &\quad \times \exp\left(-\frac{K\frac{R}{4P}\frac{E_b}{N_0}|x_i - x'_i|^2}{1+K+\frac{R}{4P}\frac{E_b}{N_0}|x_i - x'_i|^2}\right). \end{aligned} \tag{7}$$

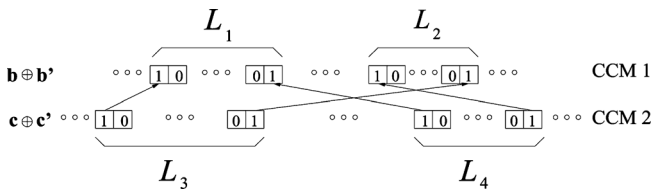

Fig. 9. Concatenated error loop structure example.

To derive an estimation for the bit error probability P_b in the error floor region, we have to take into account the dominant error events $\mathbf{e} = \mathbf{b} \oplus \mathbf{b}'$ when $E_b/N_0 \to \infty$. It was demonstrated in [18] that the error events in the uncorrelated fast flat fading channel with CSI for any individual CCM are the same as in the AWGN channel. The only change lies in the calculation of the bound itself since the PEP of the sequences $\mathbf{x}$ and $\mathbf{x}'$ (corresponding to $\mathbf{b}$ and $\mathbf{b}'$, respectively) is different for both kind of channels. Note that, in any case, the bound obtained under uncorrelated flat fast fading should converge to the bound in AWGN when $K \to \infty$.

Moreover, [14] shows that, in the case of using parallel concatenated CCM with feedback, the dominant error events in the error floor region for S-random interleavers consist in the concatenation of 2 individual binary weight 2 error loops for each CCM block. The structure of the binary error loops is $100\cdots001$, and has a minimal length L_{min} depending on the kind of CCM and on the quantization factor Q set. In general, $L_{min} = Q + p$, where p is a positive integer in $\{0, 1, 2\}$ depending on the CCM structure. Said error loop concatenation happens when the S factor of the interleaver is high enough $(S > 3 \times L_{min})$ to avoid the concatenation of just one error loop per CCM, which would offer very poor distance properties.

Given all this, it has been found that, in the case of using PCCCM in the uncorrelated fast flat fading channel, the same properties hold, and so a bound can be developed taking into account the concatenation of 2 individual binary weight 2 error events and their corresponding PEP. Fig. 9 depicts this situation, so that 2 error loops in $\mathbf{b}$ for CCM 1 are interleaved to 2 error loops in $\mathbf{c}$ for CCM 2. Error loop lengths $L_i, i = 1, 2, 3, 4$ account for the fact that they may not always have minimal lengths. They could exhibit lengths $L_i = m_i \cdot L_{min}, m_i$ being a positive integer greater than 0. Nonetheless, their appearance will be less likely as the cases with $L_i = L_{min}, i = 1, 2, 3, 4$ as $E_b/N_0 \to \infty$.

Therefore, a bound for the bit error probability can be written as

$$P_{b_{\text{floor}}} \approx \frac{\omega_{\min} \cdot M_{\text{loop}}}{N} \text{average}_{(\mathbf{x},\mathbf{x}'|\mathbf{e})}\{P_e(\mathbf{x} \to \mathbf{x}'|\mathbf{x})\}, \tag{8}$$

where the average is calculated numerically for all pairs $\mathbf{x}, \mathbf{x}'$ related through the mentioned kind of error events $\mathbf{e}$, and $\omega_{\min}$ is the binary weight of the errors, i.e., 4 in this case. M_{loop} is the number of loops of the kind described allowed by the permutation structure of the interleaver chosen. It is self-evident that $\mathbf{x}, \mathbf{x}'$ are only evaluated for their differing values, i.e., for the 4 error loops of lengths $L_i, i = 1, 2, 3, 4$. Note that as the CCM blocks are nonlinear and they do not comply with the uniform

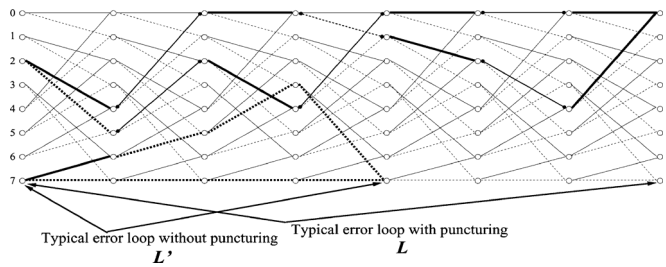

Fig. 10. Trellis of a Bernoulli shift map based CCM with $Q = 3$. Solid: transition triggered by a 0. Dotted: transition triggered by a 1. Strong boldline: path through the trellis followed by a typical error event. Weak boldline: punctured out symbol and transition.

error property (UEP) [30], for the same error loop concatenation $\mathbf{e}$ all the calculations with every possible sequence $\mathbf{x}$ have to be made. As a result, the final value of the bound depends on the previous value of x_k (among 2^Q possibilities) when the error loop starts, and also on all the possible b_j different bit information trajectories during the extent of the individual error loop. For each individual error loop with length L_i, this amounts to performing $2^{L_i} \cdot 2^Q$ calculations.

It is clear that a comprehensive bound may be quite unpractical to calculate. We will resort here to approximating the bound by the specific error loop with the minimum associated product distance, calculated as

$$d^2_{prod} = \prod_{L_1,L_2,L_3,L_4} |x_i - x'_i|^2 \tag{9}$$

This product distance is taken along the 4 possible loops of the corresponding error events. We take the product distance as a more significant quantity in the fading channel, as seen in (7), where the PEP tends to be inversely proportional to d^2_{prod} as $E_b/N_0 \to \infty$. It will be shown that this is enough to characterize the error floor region of a given PCCCM through:

$$P_{b_{\text{floor}}} > \frac{\omega_{\min} \cdot M_{\text{loop}}}{N} P_e(\mathbf{x} \to \mathbf{x}'|\mathbf{x})|_{\mathbf{x}' \neq \mathbf{x}|\min\{d^2_{prod}\}}. \tag{10}$$

Though the examination of the error loops and their role in a corresponding bound have been originally developed for the rate $R = 1/2$ bits/symbol PCCCM, all this is valid for the punctured PCCCM ($R = 1$ bits/symbol). The main change to be taken into account is the need to characterize the new loops happening in the punctured CCM. Once this is made, all the rest is straightforward. As could be expected, the error loops for the punctured CCM run through the unpunctured trellis during L steps (see Fig. 10), but contribute with distances similar to the ones corresponding to an unpunctured loop of length L', i.e., roughly $L/2$.

B. Pinch-Off Point Location Through Density Evolution

By performing iterative decoding, the convergence of the BER of a concatenated coded system to the error floor falls down abruptly around a given E_b/N_0 threshold. This value marks the so-called waterfall or pinch-off region [31]. Its location gives an approximate value for the minimum useful E_b/N_0. As a consequence, having a tool to calculate and characterize the pinch-off point is a key fact. Finding the threshold

has been traditionally done in concatenated systems through the examination of the mutual information exchange evolution of the *a posteriori* probability values at the output of each SISO decoder [32]. The mutual information I for binary data is defined and calculated as [24]

$$I = \frac{1}{2} \sum_{b=0,1} \int_{-\infty}^{\infty} p(\Lambda|b) log_2 \left(\frac{2p(\Lambda|b)}{p(\Lambda|1) + p(\Lambda|0)} \right) d\Lambda, \tag{11}$$

where $p(\Lambda|b)$ is the probability density function of the log probability estimation ratio at the input $(\Lambda = \Lambda(b;\mathrm{I}))$ or output $(\Lambda = \Lambda(b;\mathrm{O}))$ of the corresponding SISO when the bit sent takes the value b. We have dropped the index in b, and the arguments in Λ for simplicity (see Section II). Mutual information thus defined is bounded between 0 and 1. $I = 0$ means that the probability distributions $p(\Lambda|0)$ and $p(\Lambda|1)$ are not discernible, and $I = 1$, that the probability distributions have no significant overlapping.

These concepts are in the basis of the so-called EXIT charts, where the input/output mutual information characteristic for each SISO is plotted as a continuous line evolving from a minimum I value to $I = 1$ (when the encoder blocks are recursive). In AWGN, these charts are generated by feeding a Gaussian random variable (RV) as *a priori* information to the SISO decoder, together with the corresponding AWGN corrupted channel values, and numerically evaluate (11) over the SISO outputs [32]. The Gaussian hypothesis is a good approximation when using linear systems such as binary turbocodes or TTCM. In those contexts, there are small deviations from actual density evolution, and they are usually explained by the presence of the finite size interleaver and the high degree of correlation that appears between SISO inputs/outputs after some iterations.

EXIT charts have already proved their usefulness in chaos-based communications [15], specially under amplitude mapping [14]. Therefore, we are going to use them to get the approximated E_b/N_0 pinch-off thresholds. To test whether the Gaussian hypothesis holds, we show in Figs. 11 and 12 the histograms of the extrinsic data at the output of the SISO for two instances of CCM under AWGN. For clarity, we only show the values for the case $b = 1$. For 3 iterations, we can see that both histograms fit well to a Gaussian distribution. For 8 iterations, the mTM data histogram fits better to an extreme value distribution [33], while the ImTM extrinsic data values are still reasonably Gaussian distributed. Following these examples, we would expect a good agreement between EXIT charts and the mutual information evolution when using large interleavers for the ImTM case, up to number of iterations. In the case of mTM, we would expect to witness deviations after a few number of iterations.

The aforementioned situation is made evident in Fig. 13. Note that, for ImTM, both in the AWGN and flat fading case, the EXIT chart and actual mutual information evolution provide a good agreement, at least before the number of iterations leads to a situation where the correlation between SISO inputs/outputs becomes too high for the subsequent iterations to be of any use [34]. Note also how we get a clear mismatch in the mTM cases, as foreseen. This fact make the EXIT charts in this latter case not

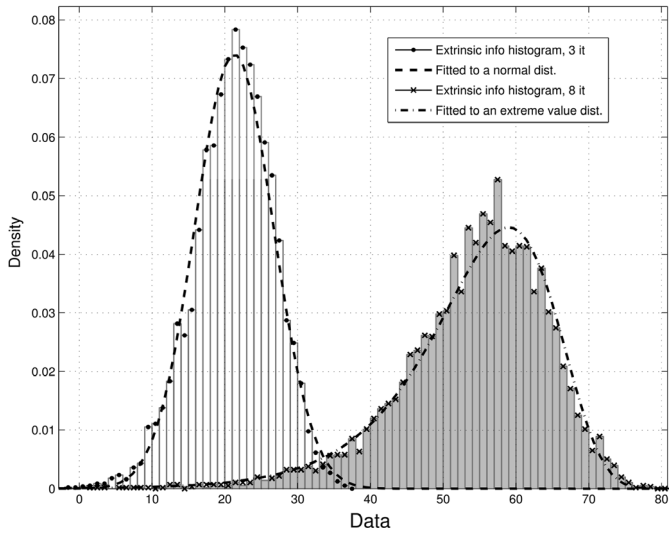

Fig. 11. Histogram of the extrinsic data for a mTM PCCCM, after 3 and 8 decoding iterations, for $E_b/N_0 = 1$ dB.

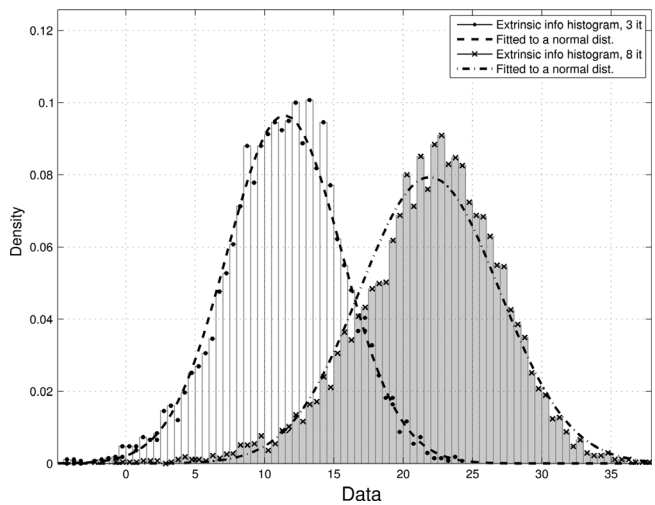

Fig. 12. Histogram of the extrinsic data for an ImTM PCCCM, after 3 and 8 decoding iterations, for $E_b/N_0 = 1$ dB.

so useful, although they still provide valuable insight. It is worth pointing out that the correlation between SISO inputs/outputs for mTM grows very fast in each iteration. The reason is that the trellis structure of said CCM has a special symmetry [35], so that not all the states are uniformly visited depending on the starting state. This in fact prevents spreading the extrinsic information efficiently through the whole sequence.

In Table I, we can see the E_b/N_0 thresholds in AWGN for some combinations of CCM blocks, as calculated through their corresponding EXIT charts. If we compare the estimated thresholds with the actual ones given by BER simulations (see Table III), we see that in many cases the differences are bounded by 0.1 dB. We consider this to be a *good agreement*. The exception are the cases involving the mTM CCM, where differences reach 0.2 dB. All the CCM in the examples, excepting mTM, have regular trellis structures and keep almost Gaussian LLRs for many iterations, and the SISO inputs/outputs correlation grows by small amounts in each decoding step.

In Table II, we provide the E_b/N_0 thresholds for the same cases, but in the Rayleigh flat fading channel $(K = 0)$. By

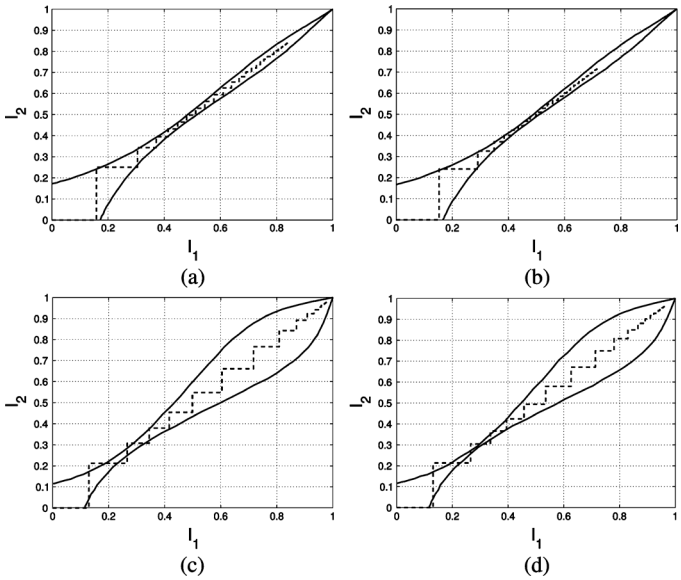

Fig. 13. EXIT charts *vs*. actual mutual information average trajectory for several PCCCM cases and environments. In all the cases, we use phase mapping, no puncturing, the quantization factor is $Q = 5$, and the interleaver chosen for the mutual information evolution simulations is an S-random interleaver with $N = 5500$ ans $S = 19$. (a) ImTM, AWGN, -0.1 dB, (b) ImTM, fad., $K = 0, (E_b)/(N_0) = 0.7$ dB, (c) mTM, AWGN, 0.1 dB, (d) mTM, fad., $K = 0, (E_b)/(N_0) = 0.8$ dB.

TABLE I
PINCH-OFF E_b/N_0 THRESHOLD (DB) IN THE AWGN CHANNEL, UNPUNCTURED PCCCM WITH PHASE MAPPING, AND QUANTIZATION FACTOR $Q = 5$

	TM	ImTM	mTM	mBSM
TM	1.0	0.2	0.4	0.1
ImTM	0.2	−0.1	−0.1	−0.1
mTM	0.4	−0.1	0.1	−0.2
mBSM	0.1	−0.1	−0.2	−0.4

TABLE II
PINCH-OFF E_b/N_0 THRESHOLD (DB) IN THE FLAT FADING CHANNEL WITH $K = 0$, UNPUNCTURED PCCCM WITH PHASE MAPPING, AND QUANTIZATION FACTOR $Q = 5$

	TM	ImTM	mTM	mBSM
TM	1.9	1.1	1.2	0.9
ImTM	1.1	0.7	0.7	0.6
mTM	1.2	0.7	0.9	0.6
mBSM	0.9	0.6	0.6	0.4

comparing these values to the ones provided by BER simulations (see Table IV), although the Gaussian hypothesis for the LLRs is not so well met now, we see that the E_b/N_0 differences are still limited to 0.1 dB. The exceptions to this are again cases where the mTM CCM is present. Note that, for growing K, we get closer and closer to a pure AWGN channel, and therefore, for the Rician flat fading channel with $0 < K < \infty$, the EXIT charts are expected to be as useful and as accurate as their AWGN only, or AWGN plus $K = 0$ flat fading counterparts.

All of this makes it evident that the EXIT charts are still a good tool to get E_b/N_0 thresholds and get valuable information for this whole kind of chaos-based systems. In the following, we are going to provide and analyze simulation results that validate our approach.

TABLE III
PINCH-OFF E_b/N_0 THRESHOLD (DB) AS IN TABLE I, CALCULATED THROUGH BER SIMULATIONS WITH BLOCK SIZE $N = 5500$

	TM	ImTM	mTM	mBSM
TM	0.9	0.2	0.2	0.1
ImTM	0.2	−0.1	−0.1	−0.2
mTM	0.2	−0.1	−0.1	−0.2
mBSM	0.1	−0.2	−0.2	−0.4

TABLE IV
PINCH-OFF E_b/N_0 THRESHOLD (DB) AS IN TABLE II, CALCULATED THROUGH BER SIMULATIONS WITH BLOCK SIZE $N = 5500$

	TM	ImTM	mTM	mBSM
TM	1.8	1.0	1.1	0.9
ImTM	1.0	0.7	0.8	0.6
mTM	1.1	0.8	0.7	0.6
mBSM	0.9	0.6	0.6	0.5

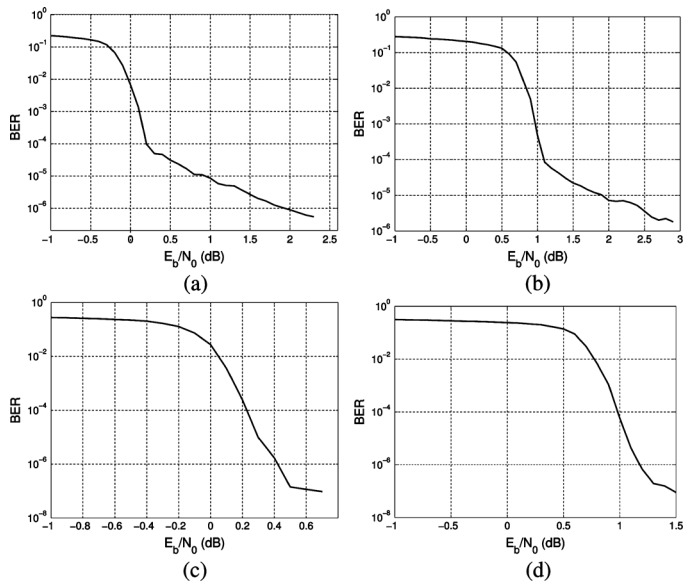

Fig. 14. BER simulations corresponding to the cases depicted in Fig. 13. (a) ImTM, AWGN. (b) ImTM, fading, $K = 0$. (c) mTM, AWGN. (d) mTM, fading, $K = 0$.

C. Accuracy of Density Evolution Analysis

In Tables I and II, we provide a set of E_b/N_0 values for the approximated location of the pinch-off point for different scenarios and different CCM combinations. To test the accuracy of the data, we have performed simulations with the systems exemplified before, setting pairs of CCMs joined by a $N = 5500$ S-random interleaver with $S = 19$. The BER results in Fig. 14 correspond to the cases whose EXIT charts are shown in Fig. 13. By analyzing these BER results, we have collected the E_b/N_0 values where the waterfall region starts, which constitute the practical pinch-off thresholds.

In Table III we can see the experimental values for the combinations of Table I. As stated, note how the absolute differences are within 0.1 dB in most cases. The small discrepancies are mainly due to the finite size interleaver, which cannot prevent the building up of the data correlation as iterations proceed. This is the reason for the progressive diminishing of the mutual information growth towards 1 as shown in the average mutual information trajectory in Fig. 13. The bigger differences involve the

mTM CCM, and are related to the non-Gaussian density evolution of its LLR values. This mismatch in AWGN is shown in Fig. 13(c), where it is easy to foresee a lower threshold than the one predicted by the EXIT charts: note how the average mutual information grows faster up to a certain point for the same E_b/N_0.

In Table IV we can verify the threshold values in Rayleigh flat fading, and compare them to the theoretical EXIT-based ones (Table II). Again, there are minor differences, explained by the finite size interleaver, and bigger differences, always involving the mTM CCM. This latter situation is as well related to said non-Gaussian LLR density evolution (recall Fig. 11). On the whole, we can say that the EXIT chart is still a useful tool to predict threshold values, and even a conservative one: see how the differences up to 0.2 dB for mTM combinations represent that the actual threshold is *lower* than the EXIT chart threshold.

IV. BER Results and Discussion

To illustrate the performance of the chaos-based systems we propose two different implementations of the PCCCM, and compare them to some accepted industry or research solutions. The first scenario consists in a PCCCM system with amplitude mapping of the chaotic samples (1), compared against binary turbocodes. The second comparison case is based on a punctured PCCCM system with phase mapping (2) tested against a TTCM system [24] with equivalent parameters.

One key feature in the soft-input soft-output algorithm for each case is the approximation made to calculate the Jacobian logarithm [36]

$$log(e^a + e^b) = max(a, b) + log(1 + e^{-|a-b|}). \qquad (12)$$

For fairness' sake, we have chosen the same standard Log-MAP approximation for all the cases (PCCCM, TTCM and binary turbocodes), where the correction term $log(1+e^{-|a-b|})$ is sampled and stored in a look-up table (LUT). We have taken 32 values evenly spaced for $|x| = |a - b|$ in $[0, 8[$, while the value for the correction term is 0 for $x \geq 8$. This has been shown to provide a good trade-off between decoding speed and accuracy [37].

A. Amplitude Mapping vs. Turbocodes

The CCM finite-state machine produces quantized samples of a chaotic sequence that belong to the [0, 1] interval. In the amplitude mapping scheme, they are rescaled within the interval $[-1, 1]$, so that this communication scheme is in fact related to a pulse-amplitude modulation setup [38]. Moreover, in absence of puncturing, the overall rate is $R = 1/2$. In this context, we have chosen instances of the UMTS and CDMA2000 turbocodes with BPSK mapping for performance comparison, in both cases with rates $R = 1/2$, 16-states constituent convolutional encoders and similar interleaver sizes. In the UMTS case, the standardized interleaver size chosen is 5114 [39], and, for CDMA2000, 6138 [40]. According to this, the PCCCM systems simulated have $Q = 4$ (16-states finite-state machine), and S-random interleavers with $S = 19$ and size $N = 5500$. In all the cases, the decoder performs up to 16 iterations. The PCCCM is built from a combination of two distinct CCMs, an mTM CCM and an ImTM CCM, since this structure has shown to provide a good trade-off between pinch-off E_b/N_0 threshold and final error floor levels.

On the other hand, both UMTS and CDMA2000 use native rate 1/3 turbocodes, so that rate 1/2 has to be got using puncturing, as defined in the corresponding standards [39], [40]. We have therefore included as well the performance of a native 1/2 binary turbocode, the duobinary one standardized in WiMAX [41]. In this case, we have chosen a frame size of 3840, which is the highest possible and the closest in magnitude order to our setup. The constituent encoder has 8 states and, according to the UMTS and CDMA2000 cases, BPSK mapping is used along with the WiMAX duobinary turbocode to offer the same spectral efficiency as PCCCM with amplitude mapping and no puncturing.

In Fig. 15, we group the BER results for $K = 20$ (almost no fading), $K = 5$ (intermediate case) and $K = 0$ (Rayleigh fading with no LOS component). We can see that, though in the case closest to the pure AWGN one the standard turbocodes outperform the PCCCM system proposed, the latter, under comparable circumstances, behaves considerably better as we get closer to the Rayleigh fading case. The WiMAX duobinary turbocode exhibits a specially good behavior at the start of the waterfall region, but its BER crosses to the right of the PCCCM plot for $K = 0$ as well. In fact, the PCCCM system loses up to some tenths of dB less than the standard systems with respect to the AWGN case. Previous results had already pointed out that the sparse distance spectra of PCCCM (due to the inherently nonlinear CCM constituent blocks) provide potential advantages under uncorrelated flat fading [18], [14]. We verify here that this property can in fact be successfully exploited to resist channel degradation as the LOS component vanishes, for example, in mobile communications. Note that this is quite a novelty respecting the usual linear systems design criteria for concatenated systems that focus mainly on minimum distance while relying on the hypothesis of error event uniformity [24]. Note also how the bounds for the error floor of the PCCCM cases depicted are quite tight, and can in fact be very helpful in analyzing and designing this kind of systems.

To further illustrate the behavior of the four systems with respect to the continuous degradation of the channel from AWGN to Rayleigh fading, we depict in Fig. 16 the E_b/N_0 (dB) value required to reach a BER of 10^{-3} for the same systems and same setups previously described. We can see that the binary turbocodes provide similar results, with a clear advantage for the WiMAX one. The E_b/N_0 values of the binary turbocodes range from nearly 1.0 dB when $K = 20$ to circa 2.65–2.8 dB in the Rayleigh fading channel, while PCCCM evolves from 1.2 dB to 2.23 dB, crossing the UMTS and CDMA2000 turbocode plots around $K = 7$ and clearly outperforming them in 0.5 dB in the worst case scenario. The WiMAX duobinary turbocode resists better the fading degradation, but PCCCM starts outperforming it around $K = 3$, and the final PCCCM advantage is still circa 0.4 dB for $K = 0$. The evolution of the curves as $K \to 0$ evidences the comparative robustness of this kind of PCCCM under flat fading.

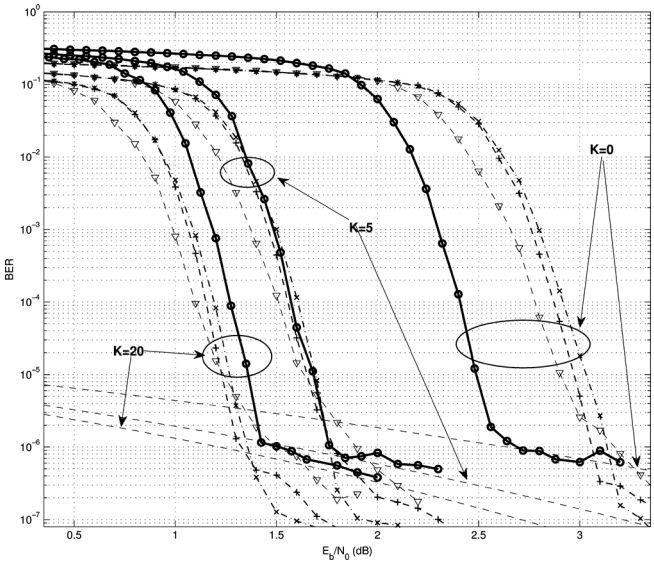

Fig. 15. Results in the Rician flat fading channel for different values of K. CDMA2000 turbocode is depicted in dashed line, "+," UMTS turbocode is depicted in dash-dotted line, "x," and WiMAX duobinary turbocode is depicted in dashed line, "v." ImTM/mTM PCCCM results are depicted in solid line, "o."

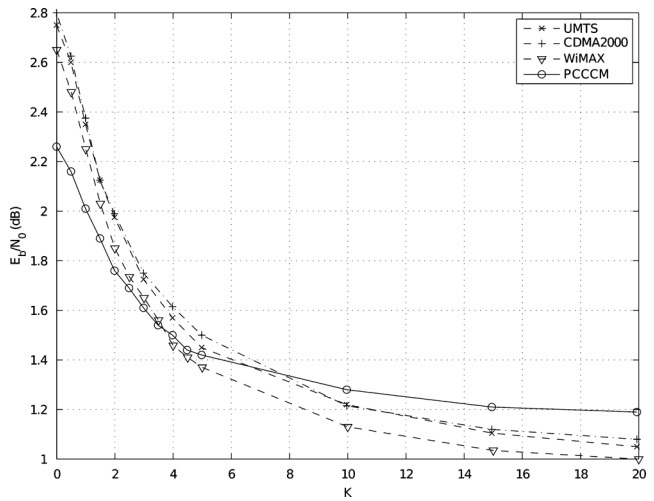

Fig. 16. E_b/N_0 (dB) needed to reach a BER of 10^{-3} for different values of K, ranging from 0 to 20.

B. Phase Mapping vs. TTCM

When using CCMs with phase mapping as constituent encoders for PCCCM, the closest equivalent concatenated system to perform comparisons with is the TTCM system with PSK modulation [42]. For the sake of fairness, we set the following parameters for the TTCM:

- 8-PSK modulation.
- $N = 5500$ bits/frame with symbol level interleaver and symbol puncturing to obtain an overall rate of $R = 1/2$.
- Two parallel 64-states convolutional encoders.
- Random interleaver at bit level.
- Approximated Log-MAP SISO decoder with 15 iterations.

The spectral efficiency obtained with this configuration is one symbol per bit on the channel (i.e.: the symbol rate matches the bit rate). The generator polynomials for the TTCM tested are, in octal form, [117 26] [43].

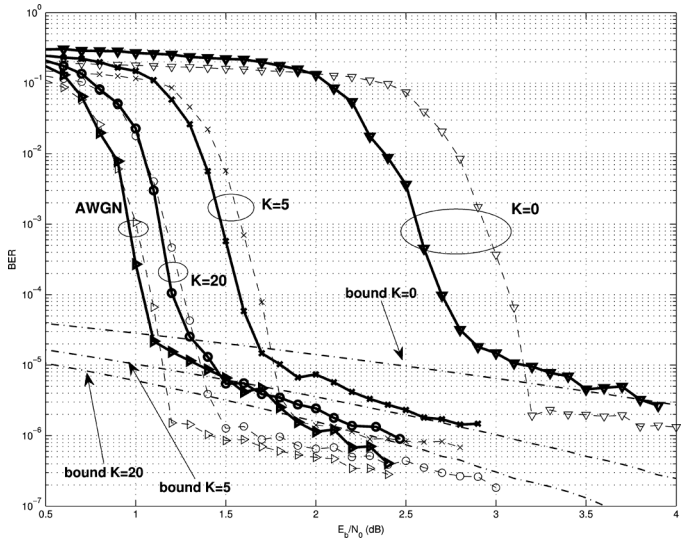

Fig. 17. BER results in the flat fading channel for different values of K. TTCM (dashed line) is compared with the ImTM/ImTM punctured PCCCM system (solid boldline) of same spectral efficiency. Bounds are depicted in dash-dotted line.

For the PCCCM, as we use puncturing, we adapt the SISO algorithm to cope with the missing symbols during iterative decoding. The approach taken is as mentioned in Section II. The setup parameters are basically the same as in the previous scenario. We reuse the $N = 5500, S = 19$ S-random interleaver. The quantization factor is now chosen as $Q = 5$. All the previous work on CCM has shown that, when $Q \geq 4$, the results are basically the same. This insensitivity to the quantization factor is convenient from the point of view of analysis, but, in practice, this means that there is no expected gain with large Q values. So $Q = 5$ and 32-states CCMs is all the same a fair comparison setup.

In Figs. 17 and 18 the systems are compared under Rician uncorrelated fast flat fading, with different K values. Note the different trade-offs provided by the ImTM/ImTM and by the ImTM/mTM setups. In Fig. 17, we can see that the ImTM/ImTM system has an E_b/N_0 pinch-off threshold quite similar to the TTCM one under AWGN, but the former behaves neatly better as K decreases. Nevertheless, the error floor is kept quite high. Note how the bounds, calculated according to the previously detailed principles, give a good estimation of the final error floor location and the corresponding slope.

In Fig. 18, we can see how the ImTM/mTM PCCCM is slightly worse than the TTCM system for AWGN, but it improves moderately as $K \to 0$. On the other hand, the resulting error floor takes fairly lower values. The bound is not so tight as before, though it can help to locate a convenient upper asymptote. The reason for the mismatch is related to the fact that the distance spectrum of mTM is much sparser than the ImTM one, so that the bound based on minimum distance values overestimates the actual result. Nevertheless, as in the case of the mTM deviations in the EXIT charts, the results obtained are still useful to help in design and evaluation tasks.

In Fig. 19, we have depicted the frame error rate (FER) results for the same test cases considered in Figs. 17 and 18. We can see here some interesting features that help to complete the

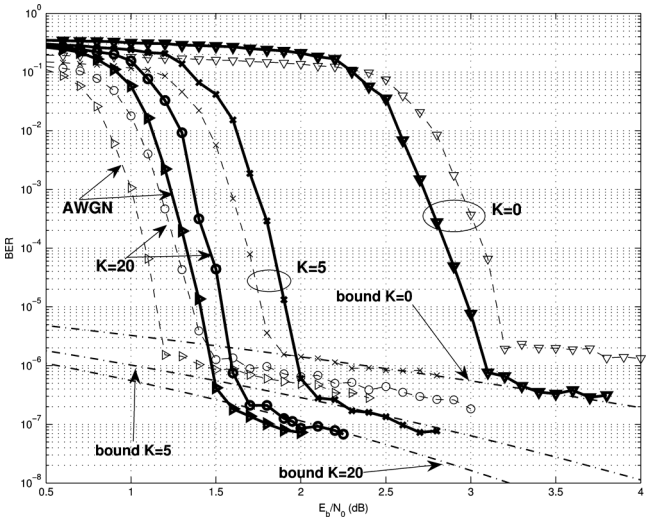

Fig. 18. BER results in the flat fading channel for different values of K. TTCM (dashed line) is compared with the ImTM/mTM punctured PCCCM system (solid boldine) of same spectral efficiency. Bounds are depicted in dash-dotted line.

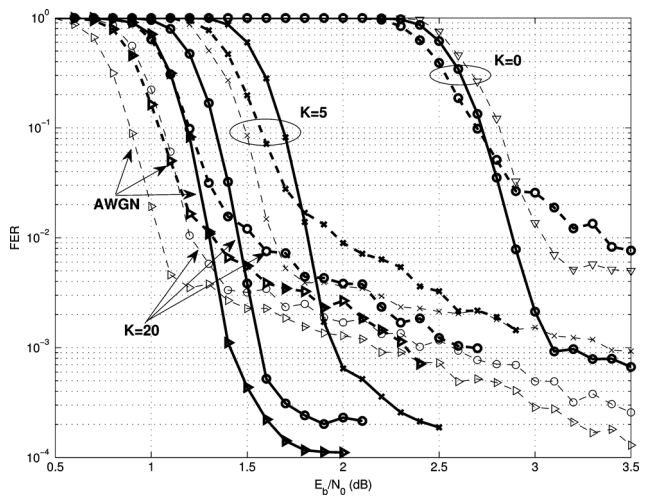

Fig. 19. FER results in the flat fading channel for different values of K. TTCM results (dashed thin line) are compared with ImTM/ImTM punctured PCCCM system results (dashed boldline), and with ImTM/mTM punctured PCCCM system results (solid boldine).

information given by the BER plots. The ImTM/ImTM PCCCM FER results fail to overrun the TTCM FER results for AWGN, $K = 20$ and $K = 5$ as seen before for the BER. This is due to the fact that the number of bit errors per frame is larger for the ImTM/ImTM PCCCM system than for the TTCM one, at least until the systems are well within the error floor region, where the BER and FER trends are quite similar (meaning a similar number of bit errors per frame). Nevertheless, this situation improves for the worst fading scenario, $K = 0$, where the chaos-based system outperforms TTCM in the waterfall region. In the case of the ImTM/mTM setup, its FER follows closely the trends of the BER plots as compared with the TTCM results, showing that they keep an equal rate of bit errors per frame throughout the waterfall and the error floor regions.

C. Discussion

In the last sections, we have been disclosing the use of tools to delve into the characteristic parameters of parallel concatenated systems under iterative decoding: the E_b/N_0 pinch-off point, and the final error floor level. We have adapted such tools for a whole class of chaos-based systems, and the analysis and simulations show that they are ready to be systematically employed in the evaluation and design tasks when chaos-based coded modulations are involved. It is true that there are some mismatches, specially in the presence of CCM blocks with complex internal structure (e.g., mTM), but, in the overall, EXIT charts and bounds, both in pure AWGN or with uncorrelated fast flat fading channels, allow a good estimation of the usable zone of a PCCCM system under possible BER *vs*. E_b/N_0 constraints.

On the other hand, the results obtained validate some important improvements introduced with respect to previous research work in PCCCM systems. The use of phase mapping as opposed to simple amplitude mapping has shown to lead to very low E_b/N_0 pinch-off points (see Tables I–IV), very remarkable indeed for a $R = 1/2$ rate concatenated system [24]. This, in turn, has provided a large E_b/N_0 margin to trade-off with spectral efficiency by using puncturing. The BER results compare successfully with TTCM equivalent systems, specially in the fading channel, while the FER results give further trade-offs and limits to be taken into account when designing PCCCM systems. These in general seem to be very robust against dispersive phenomena like flat fading. The main inconvenient is their requirement of higher computational resources [35], but the gains obtained can in fact be worth it.

As a consequence of all of this, we envisage that this kind of chaos-based communication systems can find a direct application in current leading-edge communications systems. In 4G standards for example, the extensive use of the OFDM scheme in the air interface to split a large bandwidth into orthogonally separated one-tap equalizable narrowband subchannels is a key scenario where, under sufficient depth symbol scrambling, the modulated symbols on any subchannel would essentially be affected by uncorrelated fast flat fading [44]. Therefore, we think that the next step will be to evaluate and analyze the kind of systems presented here in the 4G-like MIMO-OFDM environment and prove its usefulness and feasibility. On the other hand, the concept of Adaptive Coding and Modulation (ACM) [45] is gaining momentum in current technology developments, specially in satellite communications. The features of PCCCM presented here, such as a flexible way of combining coding and modulation with different performances and trade-offs, makes it also a good alternative in contexts where ACM is being applied.

V. Conclusion

In this article, we have introduced a new kind of parallel concatenated chaos-based systems by the addition of phase mapping to the chaotic-like output samples, and we have evaluated the possibilities of improving the resulting spectral efficiency by using puncturing. We have shown that the different alternatives, with phase or amplitude mapping, with or without puncturing, are competitive as compared with other standard systems in the Rician uncorrelated fast flat fading channel. This is explained by the fact that chaos-based coded modulated schemes, due to their

sparser distance spectra, provide a natural way to take advantage of the principle of reducing error multiplicities rather than just focusing on providing higher minimum distance values.

We have as well extended the EXIT chart and bounding tools already used successfully in previous parallel concatenated chaos-based systems to the new contexts introduced here and we have illustrated their usefulness. This casts a solid ground for future developments in chaos-based communication systems, as we can progressively rely more and more on systematic and less ad-hoc principles. These tools and the simulation results have provided a valuable insight into the possibilities and trade-offs inherent to PCCCM systems, and we are confident that they are ready to help chaos-based communications to abandon their niche place in the field, and become useful alternatives in next generation advanced communication systems.

ACKNOWLEDGMENT

The authors acknowledge financial support from the Spanish Ministerio de Ciencia e Innovación, and from Spanish Ministerio de Economía y Competitividad.

REFERENCES

[1] S. Hayes, C. Grebogi, and E. Ott, "Communicating with chaos," *Phys. Rev. Lett.*, vol. 70, no. 20, pp. 3031–3034, May 1993.

[2] M. P. Kennedy, R. Rovatti, and G. Setti, *Chaotic Electronics in Telecommunications*. Boca Raton, FL, USA: CRC, 2000.

[3] W. M. Tam, F. C. M. Lau, and C. K. Tse, *Digital Communications With Chaos*. Oxford, U.K.: Elsevier, 2007.

[4] K.-W. Wong and C.-H. Yuen, "Embedding compression in chaos-based cryptography," *IEEE Trans. Circuits Syst. II, Exp. Briefs*, vol. 55, no. 11, pp. 1193–1197, Nov. 2008.

[5] K.-W. Wong, Q. Lin, and J. Chen, "Simultaneous arithmetic coding and encryption using chaotic maps," *IEEE Trans. Circuits Syst. II, Exp. Briefs*, vol. 57, no. 2, pp. 146–150, Feb. 2010.

[6] Y. Xia, C. K. Tse, and F. C. M. Lau, "Performance of differential chaos-shift-keying digital communication systems over a multipath fading channel with delay spread," *IEEE Trans. Circuits Syst. II, Exp. Briefs*, vol. 51, no. 12, pp. 680–684, Dec. 2004.

[7] L. Wang, C. Zhang, and G. Chen, "Performance of an SIMO FM-DCSK communication system," *IEEE Trans. Circuits Syst. II, Exp. Briefs*, vol. 55, no. 5, pp. 457–461, May 2008.

[8] R. Vali, S. Berber, and S. K. Nguang, "Accurate performance analysis of chaos-based code tracking in presence of multipath fading," *Electron. Lett.*, vol. 48, no. 4, pp. 238–240, Feb. 2012.

[9] G. Kaddoum and F. Gagnon, "Performance analysis of STBC-CSK communication system over slow fading channel," *Signal Process.*, vol. 93, no. 7, pp. 2055–2060, Jul. 2013.

[10] G. Cimatti, R. Rovatti, and G. Setti, "Chaos-based spreading in DS-UWB sensor networks increases available bit rate," *IEEE Trans. Circuits Syst. I, Reg. Papers*, vol. 54, no. 6, pp. 1327–1339, Jun. 2007.

[11] G. Mazzini, G. Setti, and R. Rovatti, "Chip pulse shaping in asynchronous chaos-based DS-CDMA," *IEEE Trans. Circuits Syst. I, Reg. Papers*, vol. 54, no. 10, pp. 2299–2314, Oct. 2007.

[12] F. Arguello, D. Heras, and M. Boo, "GPU detectors for interference cancellation in chaos-based CDMA communications," *Electron. Lett.*, vol. 46, no. 10, pp. 727–729, May 2010.

[13] S. Kozic, T. Schimming, and M. Hasler, "Controlled one- and multi-dimensional modulations using chaotic maps," *IEEE Trans. Circuits Syst. I, Reg. Papers*, vol. 53, pp. 2048–2059, Sep. 2006.

[14] F. J. Escribano, S. Kozic, L. López, M. A. F. Sanjuán, and M. Hasler, "Turbo-like structures for chaos coding and decoding," *IEEE Trans. Commun.*, vol. 57, no. 3, pp. 597–601, Mar. 2009.

[15] S. Kozic and M. Hasler, "Low-density codes based on chaotic systems for simple encoding," *IEEE Trans. Circuits Syst. I, Reg. Papers*, vol. 56, no. 2, pp. 405–415, Feb. 2009.

[16] F. J. Escribano, L. López, and M. A. F. Sanjuán, "Improving the performance of chaos-based modulations via serial concatenation," *IEEE Trans. Circuits Syst. I, Reg. Papers*, vol. 57, no. 2, pp. 448–459, Feb. 2009.

[17] H. Yang and G.-P. Jiang, "Reference-modulated DCSK: A novel chaotic communication scheme," *IEEE Trans. Circuits Syst. II, Exp. Briefs*, vol. 60, no. 4, pp. 232–236, Apr. 2013.

[18] F. J. Escribano, L. López, and M. A. F. Sanjuán, "Chaos coded modulations over rayleigh and rician flat fading channels," *IEEE Trans. Circuits Syst. II, Exp. Briefs*, vol. 55, no. 6, pp. 581–585, Jun. 2008.

[19] F. J. Escribano, L. López, and M. A. F. Sanjuán, "Analysis of chaos-based coded modulations under intersymbol interference," *J. Comput.*, vol. 5, no. 10, pp. 1459–1467, Oct. 2010.

[20] D. R. Frey, "Chaotic digital encoding: An approach to secure communication," *IEEE Trans. Circuits Syst. II, Exp. Briefs*, vol. 40, no. 10, pp. 660–666, Oct. 1993.

[21] C. Vladeanu, S. El Assad, J.-C. Carlach, and R. Quéré, "Improved frey chaotic digital encoder for trellis-coded modulation," *IEEE Trans. Circuits Syst. II, Exp. Briefs*, vol. 56, no. 6, pp. 509–513, Jun. 2009.

[22] Z.-H. Cai, M. Cao, and K. R. Subramanian, "Enhancement of ADSL design through concatenated coding," *Signal Process.*, vol. 81, no. 10, pp. 2187–2199, Oct. 2001.

[23] E. Krouk and S. Semenov, *Modulation and Coding Techniques in Wireless Communications*. Chichester, U.K.: Wiley, 2011.

[24] C. B. Schlegel and L. C. Pérez, *Trellis and Turbo Coding*. New York: Wiley, 2004.

[25] E. Biglieri, J. Proakis, and S. Shamai, "Fading channels: Information-theoretic and communications aspects," *IEEE Trans. Inf. Theory*, vol. 44, pp. 2619–2692, Oct. 1998.

[26] D. Divsalar and F. Pollara, "Turbo codes for PCS applications," in *Proc. Int. Conf. Commun.*, Seattle, WA, USA, Jun. 1995, vol. 1, pp. 54–59.

[27] M. K. Simon and M.-S. Alouini, *Digital Communications Over Fading Channels*. Hoboken, NJ, USA: Wiley, 2005.

[28] A. Hof, "Distance spectrum calculation of symbol punctured trellis coded modulation," in *IEEE 65th Veh. Technol. Conf. (VTC2007 Spring)*, Dublin, Ireland, pp. 1747–1751.

[29] P. Robertson and T. Wörz, "Bandwidth-efficient turbo trellis-coded modulation using punctured component codes," *IEEE J. Sel. Areas Commun.*, vol. 16, no. 2, pp. 206–218, Feb. 1998.

[30] G. Ungerboeck, "Channel coding with multilevel/phase signals," *IEEE Trans. Inf. Theory*, vol. IT-28, no. 1, pp. 55–67, Jan. 1982.

[31] S. Benedetto and G. Montorsi, "Unveiling turbo codes: Some results on parallel concatenated coding schemes," *IEEE Trans. Inf. Theory*, vol. 42, no. 2, pp. 409–429, Mar. 1996.

[32] S. ten Brink, "Convergence behavior of iteratively decoded parallel concatenated codes," *IEEE Trans. Commun.*, vol. 49, no. 10, pp. 1727–1737, Oct. 2001.

[33] A. Papoulis and S. U. Pillai, *Probability, Random Variables and Stochastic Processes*. Boston, MA, USA: McGraw-Hill, 2002.

[34] S. B. Korada and R. L. Urbanke, "Exchange of limits: Why iterative decoding works," *IEEE Trans. Inf. Theory*, vol. 57, no. 4, pp. 2169–2187, Apr. 2011.

[35] A. Wagemakers, F. J. Escribano, L. López, and M. A. F. Sanjuán, "Competitive decoders for turbo like chaos-based systems," *IET Commun.*, vol. 6, no. 10, pp. 1278–1283, Jul. 2012.

[36] S. Benedetto, D. Divsalar, G. Montorsi, and F. Pollara, "A soft-input soft-output APP module for iterative decoding of concatenated codes," *IEEE Commun. Lett.*, vol. 1, no. 1, pp. 22–24, Jan. 1997.

[37] W. J. Gross and P. G. Gulak, "Simplified MAP algorithm suitable for implementation of turbo decoders," *Electron. Lett.*, vol. 34, no. 16, pp. 1577–1578, Aug. 1998.

[38] J. G. Proakis, *Digital Communications*. Boston, MA, USA: McGraw-Hill, 2001.

[39] 3G TS.25.212 V3.3.0 (2000–06), Multiplexing and Channel Coding (FDD), Technical Specification Group Radio Access Network, 3rd Generation Partnership Project.

[40] 3GPP2 C.S0002-D Version 1.0, Physical Layer Standard for cdma2000 Spread Spectrum Systems, Revision D, Third Generation Partnership Project 2 (3GGP2).

[41] *Air Interface for Fixed and Mobile Broadband Wireless Access Systems*, IEEE Std. 802.16-2005, Part 16, IEEE 802.16 Working Group.

[42] P. Robertson and T. Wörz, "Turbo Trellis Coded Modulation (TTCM) Employing Parity Bit Puncturing and Parallel Concatenation," in *Wiley Encyclopedia of Telecommunications*. New York: Wiley, 2002, pp. 1–38.

[43] L. L. Hanzo, Y. Akhtman, L. Wang, and M. Jiang, *MIMO-OFDM for LTE, WIFI and WIMAX: Coherent Versus Non-Coherent and Cooperative Turbo-Transceivers*. New York: Wiley, 2011.

[44] S. Sesia, *LTE—The UMTS Long Term Evolution: From Theory to Practice*. Hoboken, NJ, USA: Wiley, 2011.

[45] H. Bischl *et al.*, "Adaptive coding and modulation for satellite broadband networks: From theory to practice," *Int. J. Satellite Commun. Netw.*, vol. 28, no. 2, pp. 59–111, 2010.

Francisco J. Escribano received his degree in telecommunications engineering at ETSIT-UPM, Spain, and his Ph.D. degree at Universidad Rey Juan Carlos, Spain.

He is currently Associate Professor at the Department of Signal Theory and Communications of Universidad de Alcalá de Henares, Spain, where he is involved in several undergraduate and master courses in telecommunications engineering. He has been Visiting Researcher at the Politectnico di Torino, Italy, and at the EPFL, Switzerland. His research activities are focused on communications systems and information theory, mainly on the topics of channel coding, modulation and multiple access, and on the applications of chaos in engineering.

Alexandre Wagemakers received the telecommunication engineering degree in 2003 from the Polytechnic University in Madrid, Spain, and the Ph.D. degree in applied physics in 2008 from the University Rey Juan Carlos, Madrid, where he is working as an Assistant Professor in the Department of Physics. His interest are currently the theory and applications of nonlinear dynamics.

Miguel A. F. Sanjuán received the B.S. degree in physics from the University of Valladolid, Valladolid, Spain, in 1981, and the Ph.D. degree in physics from the National University at a Distance, Madrid, Spain, in 1990.

He was a Visiting Research Associate with the Institute of Physical Science and Technology, University of Maryland at College Park, from July 1995 to September 1996. He was a Visiting Researcher with the University of Tokyo, Tokyo, Japan, in February 2002. Since 2002, he has been a Full Professor of Physics with the Universidad Rey Juan Carlos, Madrid, where he is the Head of the Departamento de Física and Head of the Nonlinear Dynamics, Chaos and Complex Systems Group.

Dr. Sanjuán is a Japan Society for the Promotion of Science Fellow. In 2008, he was elected as a Foreign Member of the Lithuanian Academy of Sciences. Associate Editorial Board Member of ten international journals in Nonlinear Dynamics. More than 60 invited lectures in seminars and conferences in Spain, Europe, USA, China, Japan, India, Cameroon, Mexico, Chile, Brazil, Peru, etc. He has been a Visiting Research Associate of the Institute for Physical Sciences and Technology of the University of Maryland and the University of Tokyo, Visiting Research Professor at the Beijing Jiaotong University, Visiting Professor in Kaunas Technological University, Lithuania, and Guest Professor of Lanzhou University, China.